Available online at www.sciencedirect.com
ScienceDirect
Journal of the European Ceramic Society 26 (2006) 3211–3219
www.elsevier.com/locate/jeurceramsoc

Effect of deposition parameters on the growth rate and dielectric properties of the $Ba(Sn_xTi_{1-x})O_3$ thin films prepared by radio frequency magnetron sputtering

Hong-Hsin Huang [a], Moo-Chin Wang [b,d], Chung-Yuan Chen [c], Nan-Chung Wu [c], Huey-Jiuan Lin [d,*]

[a] *Department of Electrical Engineering, Cheng Shiu University, 840 Cheng-Ching Road, Niaosung Hsiang, Kaohsiung 83342, Taiwan*
[b] *Department of Mechanical Engineering, National Kaohsiung University of Applied Sciences, 415 Chien-Kung Road, Kaohsiung 80782, Taiwan*
[c] *Department of Materials Science and Engineering, National Cheng Kung University, 1 Ta-Hsueh Road, Tainan 70101, Taiwan*
[d] *Department of Materials Science and Engineering, National United University, 1 Lien-Da, Kung-Ching Li, Miaoli 360, Taiwan*

Received 18 May 2005; received in revised form 19 September 2005; accepted 30 September 2005
Available online 18 November 2005

Abstract

The growth rate and dielectric properties of the $Ba(Sn_xTi_{1-x})O_3$ (BS_xT_{1-x}) thin films prepared by radio frequency (rf) magnetron sputtering at room temperature have been characterized as a function of deposition parameters. The BS_xT_{1-x} thin films are amorphous when deposited at low rf power (R_p = 100 and 125 W). The XRD result shows merely a single perovskite ($BaTiO_3$) structure and the intensity of reflection peaks increases with the rf power increasing from 125 to 150 and 175 W. When the BS_xT_{1-x} thin film is deposited at R_p = 150 W and room temperature, the deposition rate decreases with the increasing working pressure (W_p) and $O_2/(O_2 + Ar)$ ratio (O_r). The refractive index of the BS_xT_{1-x} thin films is between 2.1 and 2.3, which shows that the variation of working pressure is not very significant. The dielectric constant of the BS_xT_{1-x} thin films increases with the R_p increasing from 100 to 150 W and decreases above 150 W. The leakage current density of the $BS_{0.15}T_{0.85}$ thin films nearly displays the ohmic behavior when the electric field is below 50 kV/cm. The conduction mechanism of the $BS_{0.15}T_{0.85}$ thin films involves the Schottky emission (SE) and Poole–Frenkel emission (PF) models. The BS_xT_{1-x} thin film shows a ferroelectric characteristic in the polarization-electric field plot.

Keywords: Films; Dielectric properties; Ferroelectric properties; $BaTiO_3$ and titanates; Capacitors

1. Introduction

From a material viewpoint, $Ba(Sr,Ti)O_3$ (BST in short) can be categorised as a solid solution between $BaTiO_3$ (BT in short) and $SrTiO_3$ (ST in short) and expressed as xBT–$(1-x)$ST. BT is a ferroelectric material with a Curie temperature at 120 °C, while ST is a paraelectric material with a phase transition temperature of approximately −245 °C (bulk). In the past several years many studies have been carried out focusing on the deposition techniques and electrical properties of BST films.[1,2]

In recent years, thin films such as BT,[3] ST,[4] $Pb(Zr,Ti)O_3$,[5] $Ba(Zr_xTi_{1-x})O_3$,[6,7] $(Ba,Sr)TiO_3$,[8] $(Ba_{1-x}Sr_x)(Ti_{0.9}Sn_{0.1})O_3$,[9] and $(ST/Bi)_n$[10] thin multilayers with a high relative dielectric constant have been considered for use as storage capacitors in dynamic random access memories (DRAMs); such a dielectric material should have a low leakage current and a high dielectric constant, and it is desirable to have a paraelectric phase to avoid fatigue due to ferroelectric domain switching.[1]

Among the modified BT compositions, the barium stannate titanite, $Ba(Sn_xTi_{1-x})O_3$, (BS_xT_{1-x} in short, $0 < x < 1$) system has attracted considerable attention. BS_xT_{1-x} is a solid solution of barium titanite and barium stannate, $BaSnO_3$. BS_xT_{1-x} represents an interesting model system for diffuse phase transition ferroelectrics.[11] Significant deviation from the Cuire–Weiss law for $x \geqq 0.1$ has been reported by Yasuda et al.[12] Furthermore, Oh et al.[13] also have pointed out that the ferroelectric domain structure of BS_xT_{1-x} is observed for $x \leqq 0.13$, proving a long-range order in this composition range. The result of a temperature-dependent X-ray diffraction (XRD) study on $BS_{0.05}T_{0.95}$ ceramics with dielectric measurements have been

* Corresponding author. Tel.: +886 37 381702; fax: +886 37 324047.
E-mail address: hjlin@nuu.edu.tw (H.-J. Lin).

0955-2219/$ – see front matter © 2005 Elsevier Ltd. All rights reserved.
doi:10.1016/j.jeurceramsoc.2005.09.109

investigated by Muller et al.[14] and interpreted in terms of mechanically clamped tetragonal and cubic phases, coexisting in the vicinity of ferroelectric cubic–tetragonal phase transition temperature in grains with inhomogeneous Sn distribution. Recently, dielectric properties[15] and elastic behavior[16] of BS_xT_{1-x} ceramics have been discussed. Although the BS_xT_{1-x} ceramics and their properties have been reported;[11–15] however, the BS_xT_{1-x} thin film deposited on an *n*-Si(1 0 0) wafer by radio frequency (rf) magnetron sputtering on room temperature substrate has not been conducted.

In the present study, the effect of deposition parameters on the growth rate and dielectric properties of rf magnetron sputtered BS_xT_{1-x} thin films on an *n*-Si(1 0 0) wafer have been investigated using X-ray diffraction (XRD), scanning electron microscopy (SEM), energy dispersive spectrometry (EDS), automatic ellipsometry and capacitance voltage measurements. The influences of deposition parameters on the crystal structure, deposition rate, oxygen content, Sn/Ti ratio, refractive index, dielectric properties and leakage current density of the BS_xT_{1-x} thin films have been discussed in detail.

2. Experimental procedure

2.1. Thin film preparation

The chemical composition of the BS_xT_{1-x} targets is listed in Table 1. Commercial $BaTiO_3$ (purity 99.0%, supplied by Noah Tech. Co., San Antonia, TX, USA) and $BaSnO_3$ (purity 99.0%, supplied by Noah Tech. Co.) were weighed and ball-milled with acetone and alumina balls for 24 h. The mixture was dried by an infrared lamp and subsequently ground and sieved. The powders through an 80-mesh sieve was then mixed with a 1.0 wt% polyvinyl acetate binder and pressed at 180 MPa to a disk of 6.2 cm in diameter. The pressed disk was heated at 600 °C for 30 min with 4.5 °C min^{-1} to burn out the binder. After the binder was burned out, the target disk was then heated at 1330 °C for 2 h with 1.5 °C min^{-1}, and cooled to room temperature with 3 °C min^{-1}.

The substrate of a 10 mm × 10 mm × 0.5 mm *n*-Si(1 0 0) wafer was ultrasonically cleaned in trichloroethylene, acetone, and propanol[16] and followed by rinsing in deionized water several times before being loaded into the sputtering chamber. Buffer HF was used to remove native oxides on the Si surface. Finally, the cleaned Si substrate was dried by N_2.

The BS_xT_{1-x} thin films with various x values were also deposited on the Si substrate by rf magnetron sputtering. The sputtering apparatus is shown schematically in Fig. 1. The overall deposition parameters for the preparation of the BS_xT_{1-x} thin films are listed in Table 2. Before sputtering, firstly the substrate and target were put on stands and shielded by a shutter. The sputtering chamber was evacuated to 2.0×10^{-5} Torr by using rotating and oil diffusion pumps. The flow rate ratio of the sputtering gases of O_2 and Ar was set at 1:9, maintaining the working pressure at 1.0×10^{-2} Torr. The BS_xT_{1-x} target was presputtered in Ar for 20 min to clean the surface for enhanced film adhesion. The Pt top electrode with a thickness of 50 nm and a diameter of 350 μm were patterned by a shadow mask process. The Ag bottom electrode was fitted by painting the body with silver paste and drying.

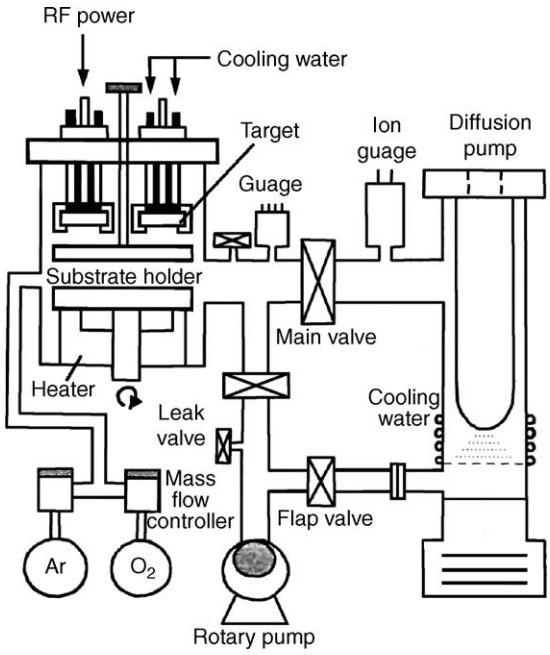

Fig. 1. Schematic diagram of the sputtering apparatus for the preparation of BS_xT_{1-x} thin films.

2.2. Films characterization

The thickness and refractive index of the BS_xT_{1-x} thin films with various x values were determined by an automatic ellipsometer (Rudolph Research Co., Flanders, NJ, USA) with a He–Ne laser (wavelength 6328 Å) as a detecting probe and a profilometer (Tencor Alpha-Step 200; San Jose, CA,

Table 1
Chemical composition of stoichiometric ceramic targets for the preparation of $Ba(Sn_xTi_{1-x})O_3$ (BS_xT_{1-x}) thin films

Starting material	Sample notation and composition (mol%)			
	BT	$BS_{0.05}Ti_{0.95}$	$BS_{0.1}Ti_{0.9}$	$BS_{0.15}Ti_{0.85}$
$BaTiO_3$	100	95	90	85
$BaSnO_3$	0	5	10	15

Table 2
RF magnetron sputtering parameters for the preparation of $Ba(Sn_xTi_{1-x})O_3$ (BS_xT_{1-x}) thin films

Target diameter (cm)	5.0
Target–substrate distance (cm)	3.6
Background pressure (10^{-5} Torr)	2
Working pressure (10^{-3} Torr)	5
Substrate temperature (°C)	25 (room temperature)
Sputtering gas	$Ar + O_2$
$O_2/(O_2 + Ar)$	1/(1 + 9)
rf Power (W)	100–175
Film thickness (nm)	800

USA). The BS_xT_{1-x} thin films had the composition range of x varying from 0 to 0.15 and the thickness remained around 800 nm.

The phase identification of the BS_xT_{1-x} targets and BS_xT_{1-x} thin films were exercised using XRD with a Cu Kα radiation and a Ni filter, operated at 30 kV, 20 mA, and the scanning rate of $0.25^\circ\,min^{-1}$ (Model Rad IIA, Rigaku Co.; Tokyo, Japan). The morphology of the surface and cross section of the BS_xT_{1-x} thin films were examined by SEM (Hitachi, Model S-4200; Tokyo, Japan). The composition was analyzed with EDS (Model Noran Vantage, Boyager, USA) employing an internal standard method.

The dielectric constant of the BS_xT_{1-x} thin films deposited at various rf powers was measured at 20 °C using an impedance analyzer (HP4192A LF, Palo Alto, CA, USA) with a thermostat (Mini-subzero MC-81, Kisnet, Japan) at applied ac voltage = 1 V and frequency = 1 kHz. The dielectric constant (ε_r) was calculated using Eg. (1):

$$\varepsilon_r = Cd(\varepsilon_0 A)^{-1} \quad (1)$$

where C is the capacitance (F), d is the film thickness (m), A is the area of the Pt top electrode (m^2), and ε_0 is the permittivity of free space ($8.854 \times 10^{-12}\,F\,m^{-1}$).

3. Results and discussion

3.1. Crystal structure and chemical composition of the BS_xT_{1-x} thin films

When the BS_xT_{1-x} thin films are deposited at $R_p = 175$ W, $W_p = 5.0 \times 10^{-3}$ Torr, $O_r = 1/(1+9)$, and room temperature, their XRD patterns are shown in Fig. 2. It indicates that all BS_xT_{1-x} thin films are crystalline. Although Olson et al.[17] have pointed out that rf-sputtered $BaTiO_3$ films are found to change from amorphous to crystalline only on the substrate surface temperature, the XRD result illustrates that the film formed below substrate temperature (S_T) = 700 °C is amorphous, while above 800 °C the crystalline film is formed. Moreover, the rf-sputtered $Ba(Zr_{0.3}Ti_{0.7})O_3$ thin films formed at $R_p = 100$ W, $W_p = 1.0 \times 10^{-2}$ Torr, $O_r = 1/(1+9)$ and $S_T = 300$ °C, the XRD results shows that the $Ba(Zr_{0.3}Ti_{0.7})O_3$ thin films are still amorphous also reported by Wang et al.[6] However, in the present study the BS_xT_{1-x} thin film even though sputtered at room temperature, and $R_p = 175$ W shows crystalline. This phenomenon is due to the high kinetic energy of the sputter-ejected species for atomic arrangement and crystallization when sputtered at high rf power and room temperature.

Since the XRD patterns of the BS_xT_{1-x} thin films with various x values have the same trend, the effect of rf power on the crystal structure of the $BS_{0.15}T_{0.85}$ thin films has been concerned. Fig. 3 illustrates the XRD patterns of the $BS_{0.15}$ $T_{0.85}$ thin films deposited at various rf powers for $W_p = 5 \times 10^{-3}$ Torr, $O_r = 1/(1+9)$ and room temperature. From Fig. 3 (a) and (b), it can be found that the $BS_{0.15}T_{0.85}$ thin films sputtered at $R_p = 100$ and 125 W are amorphous, respectively. When the rf power increases to 150 and 175 W, the (1 0 0), (1 1 0), (1 1 1), (2 0 0)

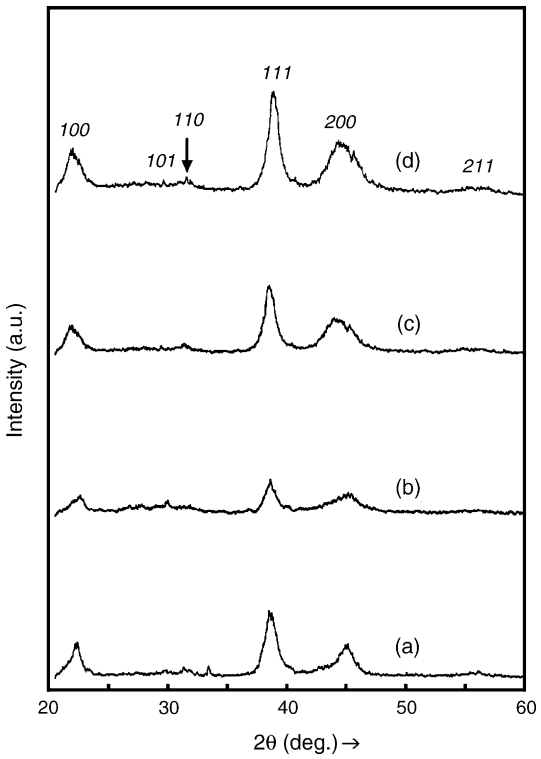

Fig. 2. XRD patterns of the BS_xT_{1-x} thin films deposited at $R_p = 175$ W, $W_p = 5 \times 10^{-3}$ Torr, $O_r = 1/(1+9)$ and room temperature: (a) $x = 0$, (b) $x = 0.05$, (c) $x = 0.1$, and (d) $x = 0.15$.

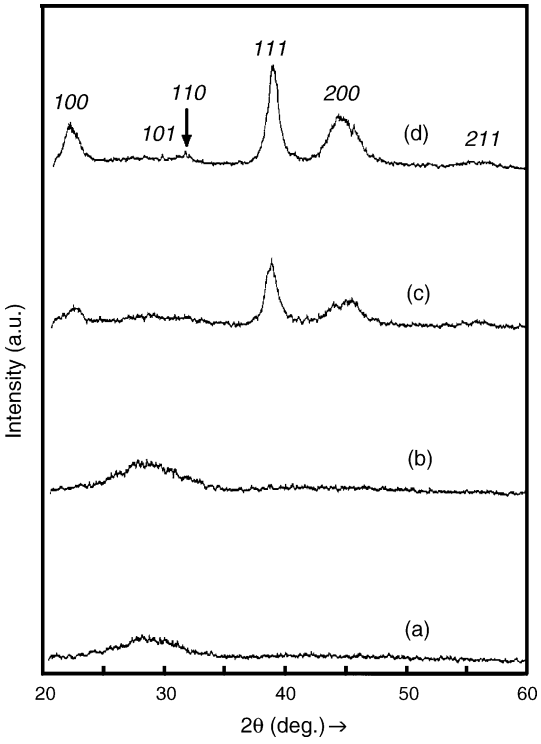

Fig. 3. XRD patterns of the $BS_{0.15}T_{0.85}$ thin films deposited at various rf powers for $W_p = 5 \times 10^{-3}$ Torr, $O_r = 1/(1+9)$ and room temperature: (a) rf = 100 W, (b) rf = 125 W, (c) rf = 150 W and (d) rf = 175 W.

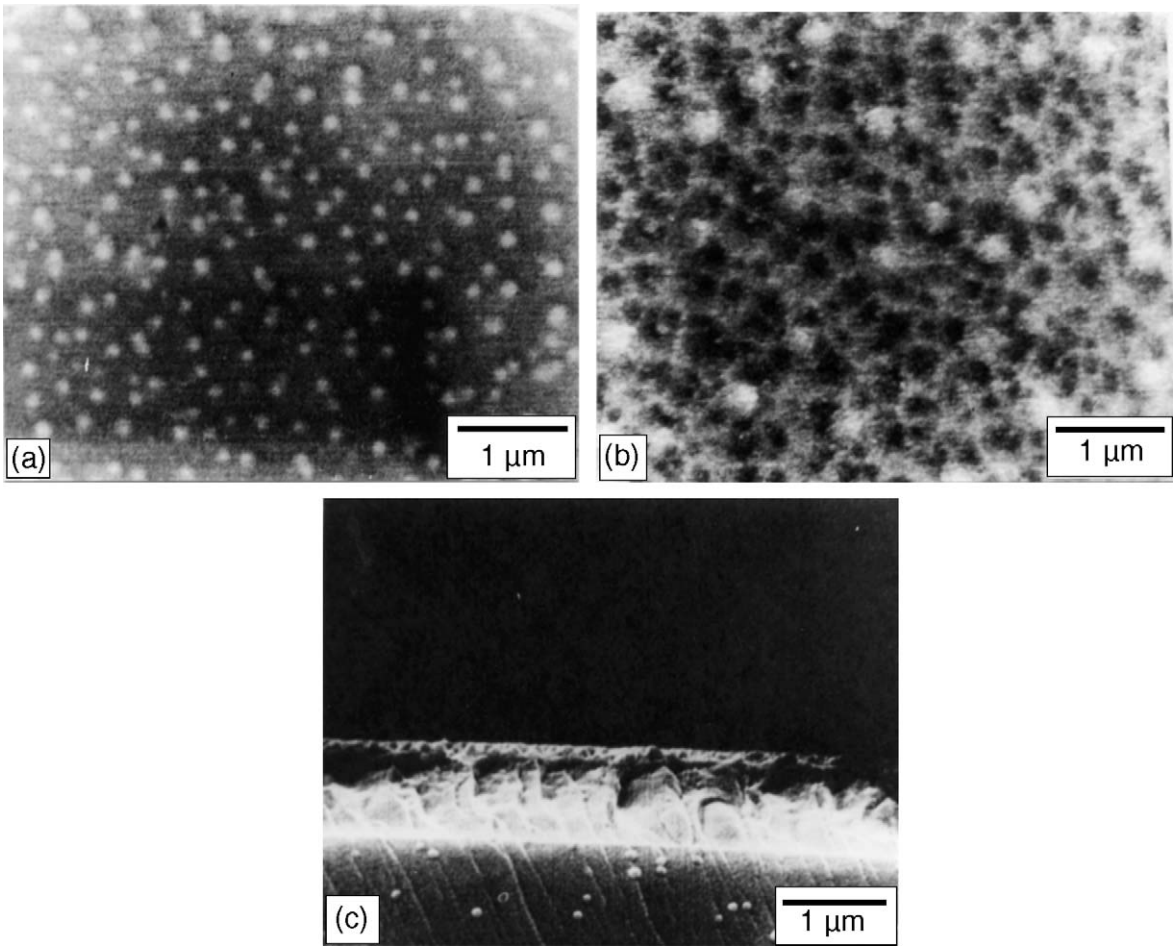

Fig. 4. SEM surface and cross-section micrographs of the $BS_{0.15}T_{0.85}$ thin films deposited at $W_p = 5 \times 10^{-3}$ Torr, $O_r = 1/(1+9)$, room temperature and different rf powers: (a) 125 W, (b) 175 W and (c) 175 W.

and (2 1 1) reflections of the $BS_{0.15}T_{0.85}$ thin films become distinct. From Fig. 3(c) and (d), it is also found that the crystallinity gradually increases with the rf power.

Fig. 3 illustrates that the crystal structure of the $BS_{0.15}T_{0.85}$ thin films still maintains the amorphous state when sputtered at $R_p = 100$ and 125 W. This phenomenon is due to the fact that the low kinetic energy of the sputter-ejected species is not sufficient for the arrangement and crystallization of atoms on the substrate when sputtered at lower rf power[18] on an unheated substrate. Moreover, the $BS_{0.15}T_{0.85}$ thin films transforms from amorphous to a single perovskite structure and the intensity of reflections increases with the rf power increasing from 125 to 150 and 175 W, respectively. This result is caused by the increased kinetic energy of the sputter-ejected species, leading to the enhanced arrangement and crystallization of atoms on the substrate.[7,18]

The SEM micrographs of the surface of the $BS_{0.15}T_{0.85}$ thin films deposited at $W_p = 5 \times 10^{-3}$ Torr, $O_r = 1/(1+9)$, room temperature and different rf powers are shown in Fig. 4. Fig. 4(a) illustrates that the surface morphology of the $BS_{0.15}T_{0.85}$ thin films sputtered at $R_p = 125$ W. According to the result of Fig. 3, the amorphous $BS_{0.15}T_{0.85}$ thin film is obtained; however, the growth morphology which follows the Stransky–Krastanov mechanism is observed in Fig. 4(a). In Fig. 4(a), the semispherical grains of about 150 nm are found on the smooth surface because rf power is relatively low. When deposited at $R_p = 175$ W, the ion energy of gas plasma increases to enhance the bombardment on the substrate surface and resputtering phenomenon is found on the rough surface (as shown in Fig. 4(b)). Nevertheless, some semispherical grains of about 300 nm are found. With high rf power higher energy gas plasma, more atoms are sputtered from the target and these high-energy sputtered atoms migrate on the substrate surface to form high quality crystalline films, which complies with the result of the XRD analysis shown in Fig. 3. Fig. 4(c) shows the SEM micrograph of the cross section of the $BS_{0.15}T_{0.85}$ thin films prepared at $R_p = 150$ W, $W_p = 5 \times 10^{-3}$ Torr, $O_r = 1/(1+9)$ and room temperature. It is found that the films are crack-free and dense, with the thickness of 800 nm.

Hwang et al.[19] have pointed out that ZnO thin films can be deposited by rf sputtering and three growth mechanisms are obtained at 100, 120, and 150–200 W rf powers. At the low rf power the Frank-van der Merwe mechanism dominates and the smooth morphology is found. When the rf power applied is 150 W, the Stranski–Krastanov mechanism dominates and the smooth surface with semispherical grains is obtained, which is

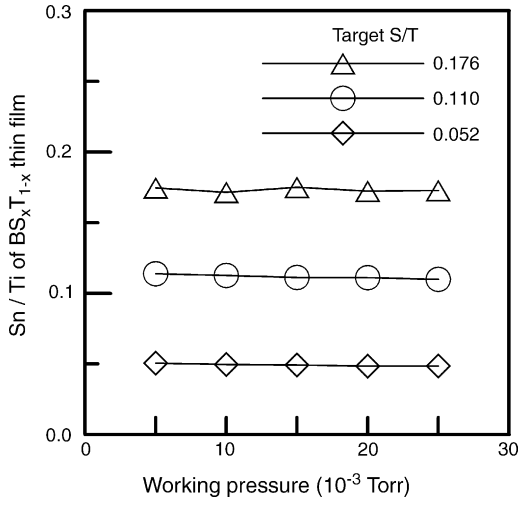

Fig. 5. Relation among Sn/Ti ratio, working pressure and Sn content (x value) in the BS_xT_{1-x} thin films with $0.05 \leqq x \leqq 0.15$ when deposited at $R_p = 150$ W, $O_r = 1{\cdot}(1+9)^{-1}$, and room temperature.

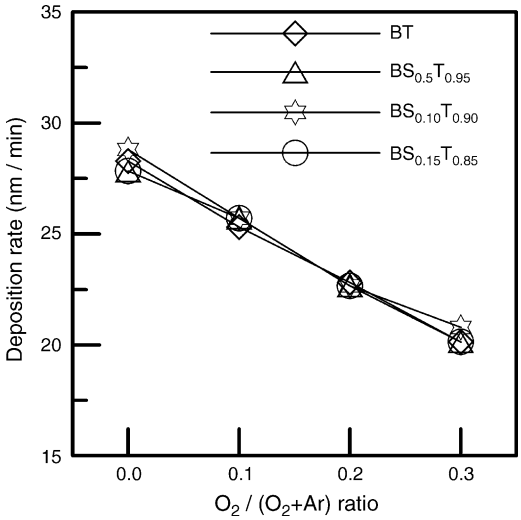

Fig. 7. Effect of $O_2/(O_2 + Ar)$ ratio on the deposition rate of the BS_xT_{1-x} thin films for $R_p = 150$ W, $W_p = 5 \times 10^{-3}$ Torr, and room temperature.

the case observed in Fig. 4(a) when deposited at the rf power of 200 W, both rough surface and resputtering are found, which is the case of Fig. 4(b).

Fig. 5 shows the relationship among the Sn/Ti ratio, W_p and Sn contents when the BS_xT_{1-x} thin films are deposited at $R_p = 150$ W, $O_r = 1/(1+9)$ and room temperature. It indicates that the $SnTi^{-1}$ ratio of the BS_xT_{1-x} thin films is yet slightly smaller than the target material. However, the effect of working pressure on the Sn/Ti ratio of the BS_xT_{1-x} thin films is not significant.

The effect of O_r and Sn content on the oxygen atom concentration of the BS_xT_{1-x} thin films sputtered at $R_p = 150$ W, $W_p = 5.0 \times 10^{-3}$ Torr and room temperature as shown in Fig. 6. It is found that the oxygen atom content in the BS_xT_{1-x} thin films increases with increasing ratio of $O_2/(O_2 + Ar)$. But the effect of $O_2/(O_2 + Ar)$ ratio on the oxygen atom content in the BS_xT_{1-x} thin films is not substantial.

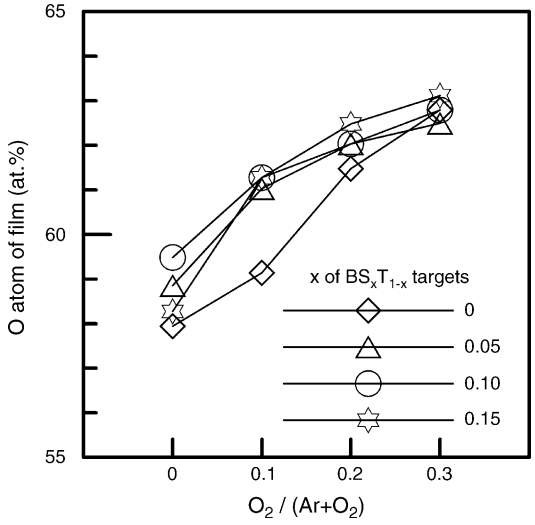

Fig. 6. Effect of the $O_2/(O_2 + Ar)$ ratio and Sn content on the oxygen atom concentration of the BS_xT_{1-x} thin films when deposited at $R_p = 150$ W, $W_p = 5 \times 10^{-3}$ Torr and room temperature.

3.2. Effect of sputtering parameters on the deposition rate of the BS_xT_{1-x} thin films

Fig. 7 shows the relation between the deposition rate and $O_2/(O_2 + Ar)$ ratio of the BS_xT_{1-x} thin films when deposited at $R_p = 150$ W, $W_p = 5.0 \times 10^{-3}$ Torr and room temperature. It illustrates that the deposition rate of the BS_xT_{1-x} thin film decreases with the $O_2/(O_2 + Ar)$ ratio.

The target position effect increases with increasing O_2 partial pressure, which reduces the energy that the particles attain to the substrate and their mobility, making it more difficult for the sputtering particles to bombard the substrate and leads to decreasing deposition rate with increasing O_2 partial pressure as reported by Sugimaya et al.[20] Moreover, Tahar et al.[21] also have pointed out that during sputtering, the target atoms are subject to collisions with ambient gas atoms and other ejected atoms resulting in a partial loss of energy and direction on their way to the substrate. The motion of both sputtered atoms and ions is thus impeded by the sputtering gas pressure. At a given rf power, the thermalizatoin region shifts toward the target by increasing O_2 partial pressure.[22] This result leads to the oxidation of the target[23,24] and possible resputtering of the film[25] and created the decreased deposition rate of the BS_xT_{1-x} thin films.

When the $R_p = 150$ W and $O_r = 1/(1+9)$, the relation between the deposition rate and working pressure is shown in Fig. 8. It is also found that the deposition rate of the BS_xT_{1-x} thin films decreases with increasing working pressure. This result is caused by the increased working pressure, which leads to the decreased mean free path of the sputtered particles. The probability of the sputtered atoms colliding with other particles in the plasma decreases when the working pressure decreases and the increased mean free path of the sputtered atoms makes those have a sufficient energy of attain to the substrate, resulting in the nucleation and growth of the film.[25]

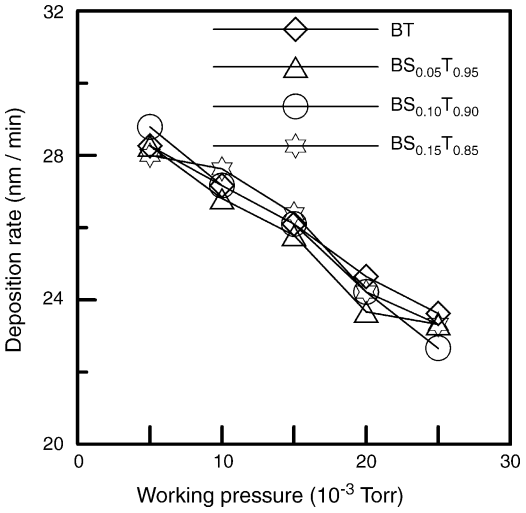

Fig. 8. Relationships among deposition rate, working pressure and Sn content for $R_p = 150$ W, $O_r = 1/(1+9)$ and room temperature.

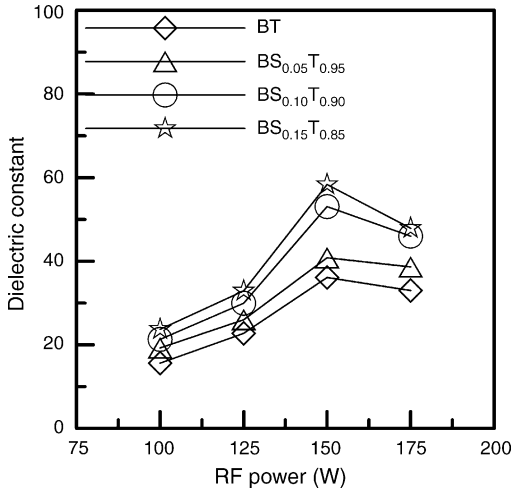

Fig. 10. Relation between rf power and dielectric constant of the BS_xT_{1-x} thin films with $0 \leqq x \leqq 0.15$ for $W_p = 5 \times 10^{-3}$ Torr, $O_r = 1/(1+9)$, deposition time = 40 min and room temperature.

3.3. Refractive index and dielectric properties of the BS_xT_{1-x} thin films

Fig. 9 shows the effect of working pressure on the refractive index of the BS_xT_{1-x} thin films sputtered at $R_p = 150$ W, $O_r = 1/(1+9)$ and room temperature. It indicates that the refractive index varies between 2.1 and 2.3, and the $BS_{0.05}T_{0.95}$ thin film has the lowest refractive index. According to Fig. 2, this result is caused by the poor crystallinity of the $BS_{0.05}T_{0.95}$ thin films than other BS_xT_{1-x} thin films. Moreover, the effect of the working pressure on the refractive index of the BS_xT_{1-x} thin films is not significant.

Furthermore, Olson et al.[17] have pointed out that the refractive index increases from 1.996 for an amorphous film to 2.400 for the most crystalline film prepared at $S_T = 1000$ °C. Pasierb et al.[26] have also pointed out that the refractive index of the well-developed perovskite structure of the $Sr_{1-x}Ba_xTiO_3$ thin films does not depend on the chemical composition (x value) but on the crystallinity difference in these films. The refractive index of the present study is consistent with the reported results of Olson et al.[17] and Pasierb et al.[26]

When the $W_p = 5.0 \times 10^{-3}$ Torr, $O_r = 1/(1+9)$, deposition time = 40 min and room temperature, the effect of rf power on the dielectric constant of the BS_xT_{1-x} thin films with various x values is shown in Fig. 10. It indicates that the dielectric constant increases with the rf power increasing from 100 to 150 W. Nevertheless, the dielectric constant decreases when the rf power increases from 150 to 175 W. The dielectric constant of the BS_xT_{1-x} thin films increases with increasing Sn content at the same rf power.

According to Fig. 3, the BS_xT_{1-x} thin films sputtered at $R_p = 100$ and 125 W still maintains the amorphous state, hence leading to the low dielectric constant. The BS_xT_{1-x} thin films sputtered at $R_p = 150$ W has the maximum deposition rate,[27] leading to the maximum dielectric constant.

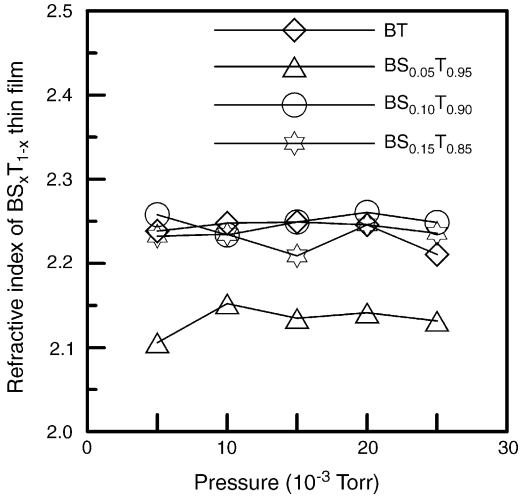

Fig. 9. Effect of working pressure on the refractive index of the BS_xT_{1-x} thin films with x values from 0.05 to 0.15 for $R_p = 150$ W, $O_r = 1/(1+9)$, and room temperature.

3.4. Effect of rf power on the leakage current density

The relation between the leakage current density and quarter power of electric field of the $Pt/BS_{0.15}T_{0.85}/Si/Ag$ capacitors, in which the $BS_{0.15}T_{0.85}$ thin films are deposited at $W_p = 5.0 \times 10^{-3}$ Torr, $O_r = 1/(1+9)$, room temperature and various rf powers are shown in Fig. 11. It is found that at the same electric field, the leakage current density increases with the rf power. At very low electric field (<50 kV/cm), the leakage current density increases approximately linearly with the electric field, i.e. the capacitors display nearly ohmic behavior. At higher electric field, varistor-like behavior is observed.[8]

Dietz et al.[8] have pointed out that the deviation of the leakage current density may be due to a slight change in microstructure or composition caused by slight variation in the processing parameters because leakage current density is very sensitive to defect microstructure and chemistry as well as to the exact nature of film-electrode interface. Furthermore, Bhattacharya

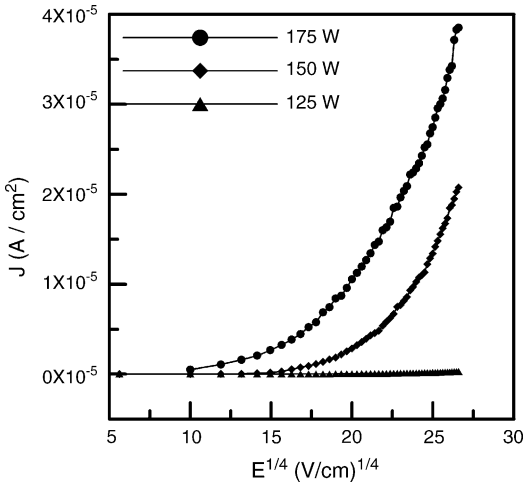

Fig. 11. Relations among leakage current density, quarter power of electric field and rf power of the Pt/$BS_{0.15}T_{0.85}$/Si/Ag capacitors in which the $BS_{0.15}T_{0.85}$ thin films are deposited at $W_p = 5 \times 10^{-3}$ Torr, $O_r = 1/(1+9)$ and room temperature.

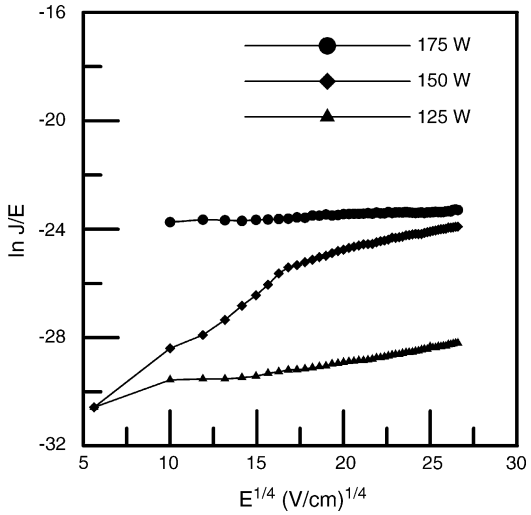

Fig. 12. Relation between log (leakage current density) and quarter power of electric field (log J vs. $E^{1/2}$) for the $BS_{0.15}T_{0.85}$ thin films deposited at $W_p = 5 \times 10^{-3}$ Torr, $O_r = 1/(1+9)$, room temperature and different rf powers.

et al.[28] also have reported that the grain boundary conduction plays one of the major roles in the leakage current characteristic, thus amorphous films are favorable for lower conduction than crystalline films. Moreover, as-deposited crystalline films may have large oxygen vacancies due to high rf power sputtering, which accelerates the ions of the sputtering plasma to strike the surface of the $BS_{0.15}T_{0.85}$ thin films and generate oxygen vacancies. Oxygen vacancy transport along the grain boundaries also increases the conductivity of the as-deposited crystalline films.

When the $BS_{0.15}T_{0.85}$ thin films is deposited at $W_p = 5.0 \times 10^{-3}$ Torr, $O_r = 1/(1+9)$, room temperature and various rf powers, the relation between log (leakage current density) and quarter power of electric field (log J versus $E^{1/4}$) of the Pt/$BS_{0.15}T_{0.85}$/Si/Ag capacitors is shown in Fig. 12. It is found that good linearity at electric field greater than 90 kV/cm

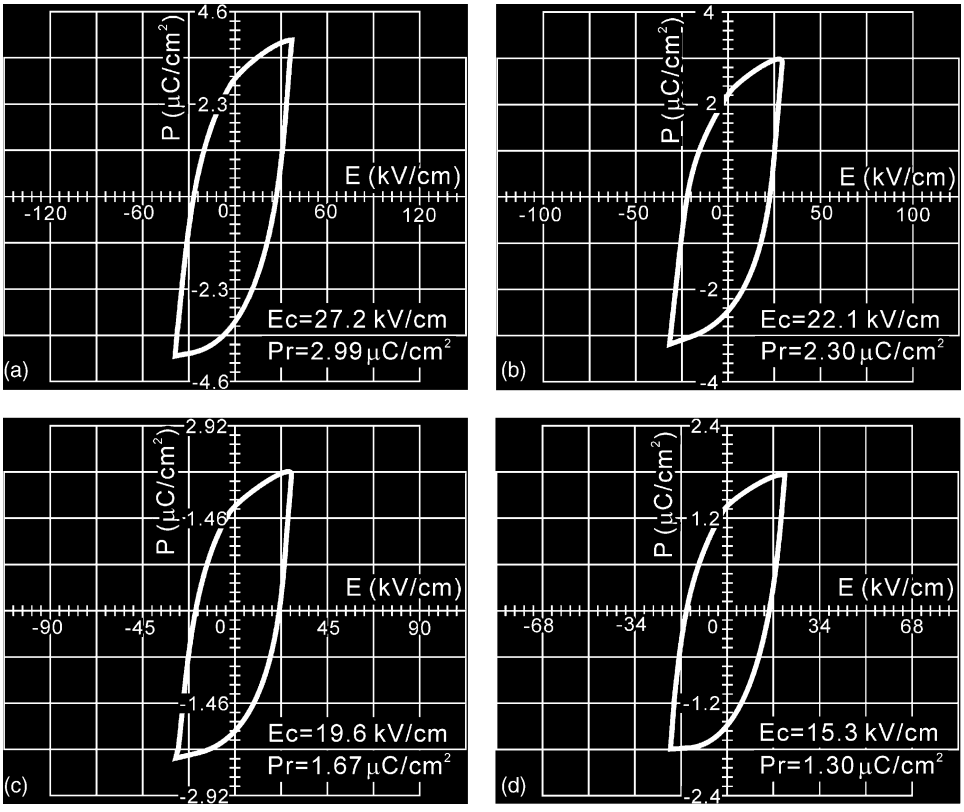

Fig. 13. Polarization vs. electric field of the Pt/BS_xT_{1-x}/Si/Ag capacitors in which the BS_xT_{1-x} thin films are deposited at $R_p = 150$ W, $W_p = 5 \times 10^{-3}$ Torr, $O_r = 1/(1+9)$ and room temperature: (a) $x = 0$, (b) $x = 0.05$, (c) $x = 0.1$, and (d) $x = 0.15$.

implies two possible conduction mechanisms of Schottky emission (SE) and Poole–Frenkel (PF) emission models.[29] Chen et al.[30] have pointed out the difference between SE and PF models is that the former is interface-controlled and the latter is bulk-controlled. If it is interface-controlled, leakage can be varied by changing the electrode material or controlling the interface state.

Moreover, the work function mismatch at the electrode interface can result in various kinds of electron emission and leakage current, such as SE, PF and tunneling emission. In general, it is not easy to distinguish among these three mechanisms.[31] On the other hand, at electric field greater than 10^6 V/cm and temperature higher than ambient, the dominant conduction is expected to be PF emission. At electric field of 10^4–10^5 V/cm and temperature of 27 °C, dominant SE mechanism has been reported.[30,31]

In the present study, the $BS_{0.15}T_{0.85}$ thin films deposited at $R_p = 125$ W have still maintained amorphous state but the crystalline film have been obtained when deposited at $R_p = 150$ and 175 W. Furthermore, the active surface increases with the rf power. This phenomenon leads to increased charged traps. Hence, the SE and PF conduction mechanisms in the $BS_{0.15}T_{0.85}$ thin films are consistent with the results of Figs. 11 and 12, and previous reports.[30,32]

Fig. 13 shows the relation between polarization versus electric field (P–E) of the Pt/BS_xT_{1-x}/Si/Ag capacitors in which the BS_xT_{1-x} thin films are deposited at $R_p = 150$ W, $W_p = 5 \times 10^{-3}$ Torr, $O_r = 1/(1+9)$ and room temperature. The clear and large hysteresis loops are obtained. This result shows the ferroelectricity of the BS_xT_{1-x} thin films. Moreover, the remnant polarization (P_r) and coercive electric field (E_c) decrease from 2.99 to 1.30 μC/cm^2 and 27.2 to 15.3 kV/cm, respectively, with x value increasing from 0 to 0.15. This result corresponds to the reported value of Oh et al.[13] Cubic $BaSnO_3$ shows paraelectricity, but tetragonal $BaTiO_3$ shows ferroelectricity. Hence, the paraelectricity of the BS_xT_{1-x} thin films increases with increasing x values. Oh et al.[13] have also pointed out that the phase transition characteristic varies from sharp to diffuse for the BS_xT_{1-x} ceramics with increasing x value, creating decreased P_r and E_c.

4. Conclusions

The $Ba(Sn_xTi_{1-x})O_3$ (BS_xT_{1-x} in short) thin films with $0 \leqq x \leqq 0.15$ have been deposited on the n-Si substrate by rf magnetron sputtering. The conclusions of this study are summarized as follows:

(1) The BS_xT_{1-x} thin films are amorphous when deposited at $R_p = 100$ and 125 W, $W_p = 5 \times 10^{-3}$ Torr, $O_r = 1/(1+9)$ and room temperature, but the single perovskite ($BaTiO_3$) structure is obtained with the rf power increasing from 125 to 150 and 175 W.

(2) The deposition rate of the BS_xT_{1-x} thin films decreases with increasing $O_2/(O_2 + Ar)$ ratio when deposited at $R_p = 150$ W and $W_p = 5 \times 10^{-3}$ Torr. Moreover, when deposited at $R_p = 150$ W and $O_r = 1/(1+9)$, the deposition rate of the BS_xT_{1-x} thin films decreases with increasing working pressure.

(3) The refractive index varies between 2.1 and 2.3 for the BS_xT_{1-x} thin films deposited at room temperature, $R_p = 150$ W, $O_r = 1/(1+9)$ and various working pressures.

(4) When deposited at $W_p = 5 \times 10^{-3}$ Torr, $O_r = 1/(1+9)$ and deposition time = 40 min, the dielectric constant increases with the rf power increasing from 100 to 150 W. The dielectric constant decreases when the rf power increases from 150 to 175 W.

(5) When the electric field is lower than 50 kV/cm, the leakage current density of the $BS_{0.15}T_{0.85}$ thin films nearly displays ohmic behavior. The conduction mechanisms of the $BS_{0.15}T_{0.85}$ thin films comprise the SE and PF emission models.

(6) The clear and large hysteresis loop shows the ferroelectricity of the BS_xT_{1-x} thin films. The P_r and E_c decrease from 2.99 to 1.30 μC/cm^2 and 27.2 to 15.3 kV/cm with the Sn content (x value) increasing from 0 to 0.15, respectively.

Acknowledgments

This work was supported by the National Science Council, Taiwan, under Contract No. NSC 92-2216-E-230-002. The authors sincerely thank Prof. M.P. Hung for manuscript discussion, Mr. J.M. Chen and Mr. S.Y. Yao for assistance in XRD and SEM.

References

1. Horikawa, T., Mikami, N., Mikita, T., Tanimura, J., Kataoka, M., Sato, K. *et al.*, Dielectric properties of (Ba,Sr)TiO_3 thin films deposited by rf sputtering. *Jpn. J. Appl. Phys.*, 1993, **32**(1), 4126–4130.
2. Baumert, B. A., Chang, L. H., Matsuda, A. T., Tsai, T. L., Tracy, C. J., Gregory, R. B. *et al.*, Characterization of sputtered barium strontium titanate and strontium titanate-thin films. *J. Appl. Phys.*, 1997, **82**, 2558–2566.
3. Hsi, C. S., Hsiao, F. Y., Wu, N. C. and Wang, M. C., Dielectric properties of the nanocrystalline barium titanite thin films deposited by RF magnetron sputtering. *Jpn. J. Appl. Phys.*, 2003, **42**(1), 544–548.
4. Wang, M. C., Hsiao, F. Y. and Wu, N. C., Characterization and leakage current density of radio frequency magnetron sputtered nanocrystalline $SrTiO_3$ thin films. *J. Cryst. Growth*, 2004, **264**, 271–277.
5. Hu, H. and Krupamidhi, S. B., Property modification of ferroelectric Pb(Zr,Ti)O_3 thin films by low-energy oxygen ion bombardment during film growth. *Appl. Phys. Lett.*, 1992, **61**, 1246–1248.
6. Wang, M. C., Chen, C. Y., Hsi, C. S. and Wu, N. C., Influence of deposition parameters on the dielectric properties of rf magnetron sputtered $Ba(Zr_xTi_{1-x})O_3$ thin films. *J. Eur. Ceram. Soc.*, 2003, **23**, 2307–2314.
7. Hsi, C. S., Chen, C. Y., Wu, N. C. and Wang, M. C., Dielectric properties of $Ba(Zr_xTi_{1-x})O_3$ thin films prepared using radio frequency magnetron sputtering. *J. Appl. Phys.*, 2003, **94**, 598–604.
8. Dietz, G. W., Schumacher, M., Waser, R., Streiffer, S. K., Basceri, C. and Kingon, A. I., Leakage current in $Ba_{0.7}Sr_{0.3}TiO_3$ thin films for ultrahigh-density dynamic random access memories. *J. Appl. Phys.*, 1997, **82**, 2359–2364.
9. Wang, M. C., Tsai, C. C., Wu, N. C. and Hung, K. M., Structure and dielectric characterization of the $(Ba_{1-x}Sr_x)(Ti_{0.9}Sn_{0.1})O_3$ thin films deposited on Pt/Ti/SiO_2/Si substrate by radio frequency magnetron sputtering. *J. Appl. Phys.*, 2002, **92**, 2100–2107.
10. Hsi, C. S., Hsiao, F. Y., Wu, N. C. and Wang, M. C., Characterization and dielectric properties of $(SrTiO_3/BaTiO_3)_n$ multilayer thin films deposited

on Pt/Ti/SiO_2/Si substrate by double rf magnetron sputtering. *Solid State Commun.*, 2003, **125**, 633–636.
11. Smolensky, G. A., Physical phenomena in ferroelectrics with diffused phase transition. *J. Phys. Soc. Jpn.*, 1970, **28**, 26–37.
12. Yasuda, N., Ohwa, H. and Asano, A., Dielectric properties and phase transitions of $BaTi_{1-x}Sn_xO_3$ solid solution. *Jpn. J. Appl. Phys.*, 1996, **35**(1), 5099–5103.
13. Oh, K. Y., Uchino, K. and Cross, L. E., Optical study of domains in $Ba(Ti,Sn)O_3$. *J. Am. Ceram. Soc.*, 1994, **77**, 2809–2816.
14. Mueller, V., Beige, H., Abicht, H. P. and Eisenschmidt, C., X-ray diffraction study revealing phase coexistence in barium titanate stannate. *J. Mater. Res.*, 2004, **19**, 2834–2840.
15. Wei, X., Feng, Y., Hang, L. and Yao, X., Dielectric relaxation behavior in barium stagnate titanate ferroelectric ceramic with diffuse phase transition. *Appl. Phys. Lett.*, 2003, **83**, 2031–2033.
16. Struube, U., Langhammer, H. T., Abicht, H. P. and Beige, H., Elastic behaviour of multilayer piezoceramic $BaTi_{1-x}Sn_xO_3$ in the lower MHz region. *J. Eur. Ceram. Soc.*, 1999, **19**, 1171–1174.
17. Olson, J. C., Stevison, D. F. and Bransky, I., The effect of temperature on properties of rf sputtered $BaTiO_3$ films. *Ferroelectrics*, 1981, **37**, 685–686.
18. Wang, M. C., Chen, C. Y., Hsi, C. S. and Wu, N. C., Characteristics and crystal structure of the $Ba(Zr_xTi_{1-x})O_3$ thin films deposited by RF magnetron sputtering. *J. Cryst. Growth*, 2002, **24**, 99–107.
19. Hwang, D.-K., Bang, K.-H., Jeong, M.-C. and Myoung, J.-M., Effects of RF power variation on properties of ZnO thin films and electrical properties of p–n homojunction. *J. Cryst Growth*, 1990, **9**, 489–492.
20. Sugiyama, K., Taniguchi, K. and Kuwabara, K., Preparation of orientated aluminum nitride films by radio-frequency reactive sputtering. *J. Mater. Sci. Lett.*, 1990, **9**, 489–492.
21. Tahar, R. B. H., Ban, T., Ohya, Y. and Takahashi, Y., Tin doped indium oxide thin films: electrical properties. *J. Appl. Phys.*, 1998, **83**, 2631–2645.
22. Leja, E., Kolodiez, A., Pisarkiewiez, T. and Stapinski, T., The dynamics of reactive ion sputtering Sn–Sb and In–Sn alloys in an Ar–O_2 atmosphere. *Thin Solid Films*, 1981, **76**, 283–287.
23. Buchanan, M., Webb, J. B. and Willams, D. F., The influence of target oxidation and growth related. Effects on the electrical properties of reactively sputtered films on tin-doped indium oxide. *Thin Solid Films*, 1981, **81**, 373–382.
24. Kester, D. J. and Messier, R., Macro-effects of resputtering due to negative in bombardment of growing thin films. *J. Mater. Res.*, 1993, **8**, 1928–1937.
25. Lee, H. C. and Lee, J. Y., Effect of sputtering pressure and nitrogen concentration on the preferred orientation of AlN thin films. *J. Mater. Sci.- Mater. Electron.*, 1994, **5**, 221–225.
26. Pasierb, P., Komormicki, S. and Radecka, M., Structural and optical properties of $Sr_{1-x}Ba_xTiO_3$ thin films prepared by rf sputtering. *Thin Solid Films*, 1998, **324**, 134–140.
27. Huang, H. H., Chen, C. Y., Lin, H. J., Wu, N. C. and Wang, M. C., Characterization of the $Ba(Sn_xTi_{1-x})O_3$ thin films prepared by radio frequency magnetron sputtering. *Mater. Sci. Eng. A*, submitted for publication.
28. Bhattacharya, P., Park, K. H. and Nishioka, Y., Control of grain structure of leaser-deposited $(Ba,Sr)TiO_3$ thin films to reduce leakage current. *Jpn. J. Appl. Phys.*, 1994, **33**(1), 5231–5234.
29. Sze, S. M., *Physics of Semiconductor Devices*. Wiley & Sons, New York, 1981, pp. 402–404.
30. Chen, X., Kingon, A. I., Al-Shareef, H. N., Bellur, K. R., Gifford, K. and Auciello, O., Leakage and interface engineering in titanate thin films for non-volatile ferroelectric memory and ulsi drams. *Integr. Ferroelectr*, 1995, **7**, 291–306.
31. Scott, J. F., Araujo, C. A., Melnick, B. M., McMillan, L. D. and Zuleeg, R., Quamtitative measurement of space-charge effects in lead zirconate-titanate memories. *J. Appl. Phys.*, 1991, **70**, 382–388.
32. Wang, D. Y. and Umeya, K., Depletion-layer dielectric properties of positive temperature coefficient of resistance barium titanate. *J. Am. Ceram. Soc.*, 1990, **73**, 1574–1581.